Structural Engineering and Mechanics, *Vol. 56, No. 4 (2015) 667-694*
DOI: http://dx.doi.org/10.12989/sem.2015.56.4.667

Optimum topology design of geometrically nonlinear suspended domes using ECBO

A. Kaveh*[1] and M. Rezaei[2]

[1]*Centre of Excellence for Fundamental Studies in Structural Engineering, Iran University of Science and Technology, Narmak, Tehran, P.O. Box 16846-13114, Iran*
[2]*Road, Building and Housing Research Center, Tehran, P.O. Box 1145-1696, Iran*

(Received September 20, 2015, Revised November 4, 2015, Accepted November 6, 2015)

Abstract. The suspended dome system is a new structural form that has become popular in the construction of long-span roof structures. Suspended dome is a kind of new pre-stressed space grid structure that has complex mechanical characteristics. In this paper, an optimum topology design algorithm is performed using the enhanced colliding bodies optimization (ECBO) method. The length of the strut, the cable initial strain, the cross-sectional area of the cables and the cross-sectional size of steel elements are adopted as design variables and the minimum volume of each dome is taken as the objective function. The topology optimization on lamella dome is performed by considering the type of the joint connections to determine the optimum number of rings, the optimum number of joints in each ring, the optimum height of crown and tubular sections of these domes. A simple procedure is provided to determine the configuration of the dome. This procedure includes calculating the joint coordinates and steel elements and cables constructions. The design constraints are implemented according to the provision of LRFD-AISC (Load and Resistance Factor Design-American Institute of Steel Constitution). This paper explores the efficiency of lamella dome with pin-joint and rigid-joint connections and compares them to investigate the performance of these domes under wind (according to the ASCE 7-05), dead and snow loading conditions. Then, a suspended dome with pin-joint single-layer reticulated shell and a suspended dome with rigid-joint single-layer reticulated shell are discussed. Optimization is performed via ECBO algorithm to demonstrate the effectiveness and robustness of the ECBO in creating optimal design for suspended domes.

Keywords: topology optimization; cable tension optimization; enhanced colliding bodies optimization; lamella dome; suspended dome; pin-joint dome; pre-stressed structure; double layer dome

1. Introduction

There are hundreds, even thousands of dome structures all over the world. No matter of their type or age, all domes rely on the same natural forces to keep them in place, and provide expansive and unobstructed space. The dome shape not only provides elegant appearance but also offers one of the most efficient interior atmospheres for human residence because the air and energy circulation are managed without obstruction. Pre-stressed space grid structure is a kind of new

*Corresponding author, Professor, E-mail: alikaveh@iust.ac.ir

http://www.techno-press.org/?journal=sem&subpage=8 ISSN: 1225-4568 (Print), 1598-6217 (Online)

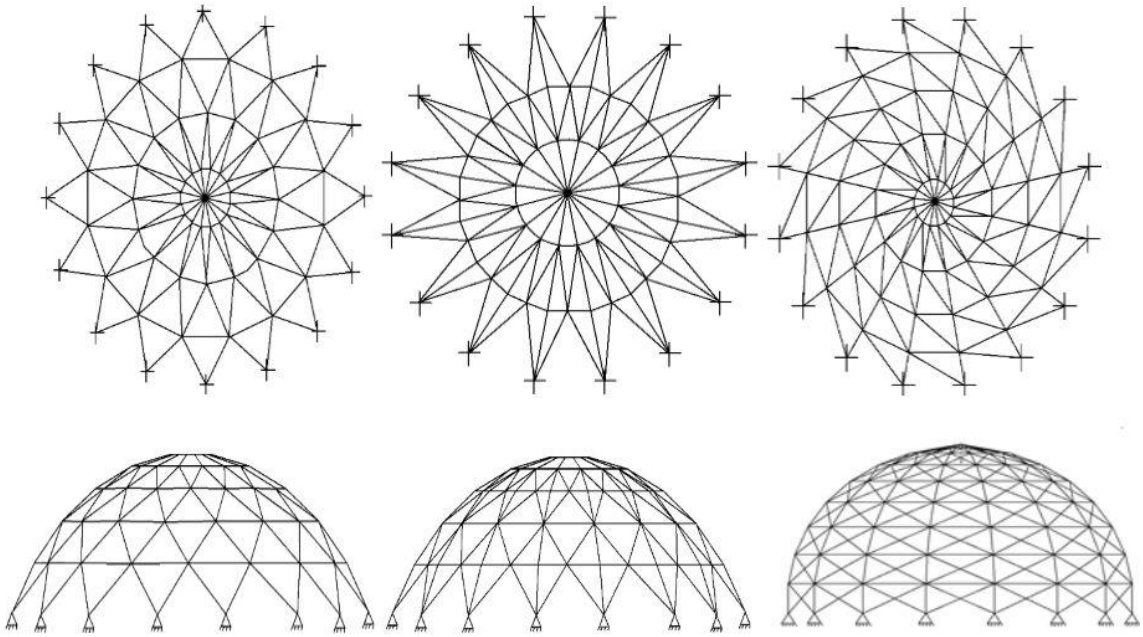

Fig. 1 Plan view and side view of a various single layer reticulated domes

structural form obtained by introducing pre-stressing technique into traditional space grid structures. Suspended dome is a new style of pre-stressed space grid structure which is formed by combing a single-layer reticulated shell and a tensegrity system (Kawaguchi *et al*. 1997, Kawaguchi *et al*. 1998). In recent years, it suspended domes have been used in some large-scale engineering structures, such as Hikarigaoka Dome in Japan and Olympic Badminton Stadium of Beijing in China. A suspended dome structure is constructed of a single-layer reticulated dome and lower tensegrity system, where the latter system consist of cable-strut elements. The single-layer reticulated dome can be chosen from single layer latticed dome such as lamella dome which has stiff element in triangle shape to provide sufficient stiffness under external loading and be stable at the same time.

The lower tensegrity system is a flexible part of suspended dome. Pre-stressing can be induced by tensioning the cables which are the flexible part of the tensegrity system. This makes the upper structure stiffer and also increases the loading capacity. Tensegrity system is made of hoop cables, radial cables and vertical struts. As it is mentioned, the cable-strut system noticeably enhances the structural properties of the many single-layer dome system such as the lamella, network, and schwedler domes (see Fig. 1). These can be used as the topmost single-layer dome of the suspended dome system. The symmetrical configuration of the lamella dome and its triangular configuration makes it quite suitable to be employed as the topmost single-layer shell of the suspended dome system. Although this paper uses single layer lamella dome for suspended dome system. The concepts of this study can be extended to other suspended dome configurations.

The basic parameters that define the geometry of a dome are the total number of rings, number of joint in each ring and height of crown, once its diameter is specified. Consequently, optimum topological design of domes necessitates treatments of these parameters as design variables. The design constraints to be considered in the formulation of the design problem can be implemented

according to one of the current design codes. Hence, in general the optimum design algorithm to be developed is expected to select tubular sections for dome members from the available list such that the provisions of the design code adopted are satisfied while the weight or cost of the dome is minimized.

Optimization methods can be divided into two general categories: (i) Mathematical programming methods that use approximation techniques to solve the optimization problem; and (ii) Metaheuristic algorithms (that mimic some natural phenomena including biology and evolution theory, Fogel *et al*. 1966, Holland 1975, Eberhart and Kennedy 1995). One of the major challenges in structural design is to introduce new meta-heuristic algorithms with higher potential and simpler usage. Popular meta-heuristic algorithms are Particle Swarm Optimization (PSO) (Eberhart RC and Kennedy 1995), Ant Colony Optimization (ACO) (Dorigo *et al*. 1996), Big Bang-Big Crunch (BB-BC) (Erol and Eksin 2006), Charged System Search (CSS) (Kaveh and Talatahari 2010a), Ray Optimization (RO) (Kaveh and Khayatazad 2012) and Dolphin Echolocation Optimization (DEO) (Kaveh and Forhoudi 2013). Successful applications of meta-heuristic algorithms in structural optimization problems have been reviewed by Saka and Geem (2013). The Colliding Bodies Optimization was recently introduced for design of structures with continuous and discrete variables (Kaveh and Mahdavai 2014). The CBO algorithm reproduces the laws of collision between bodies. Each colliding body (CB) is considered as an object with specified mass and velocity before collision; after collision, each CB moves to a new position with new velocity. Design variables can be either continuous or discrete. In real applications, cross-sectional areas are selected from a discrete list of available values (Kaveh and Talatahari 2010b). The design optimization of geometrically nonlinear geodesic domes is carried out where the design algorithm developed determines the optimum height of the crown as well as the optimum tubular steel sections for its members (Saka 2007). In this paper optimum topology design of linear elastic geodesic domes is presented. The design algorithm determines the optimum number of rings, the optimum height of crown, and tubular sections for the geodesic domes. The optimum topology design algorithm based on the hybrid Big Bang-Big Crunch optimization method is presented for the Schwedler and Ribbed domes in Kaveh and Talatahari (2010b). A comparative study is carried out for the optimum design of different types of single layer latticed domes in Kaveh and Talatahari (2010c). In this paper the optimum geometry and topology design of geodesic domes is obtained by utilizing charged system search (CSS). Liu *et al*. (2012) analyzed the effect of temperature change during pre-stressing construction on pre-stressing force in cables. Moreover, a new pretension control method and a simplified calculation formula were proposed and verified for suspended dome structures.

The elliptic paraboloid suspended dome, whose span is 110 m×80 m and height is 9.4 m, is employed in the steel roof of Houjie Gymnasium (Jiang 2013). In Kocieck and Adeli (2013), a two-phase GA approach is suggested for weight optimization of free-form steel space-frame roof structures consisting of rectangular hollow structural sections (HSS). Two roof structures which are subjected to the AISC LRFD code and ASCE-10 loadings were optimized. An efficient methodology is proposed for optimal design of large-scale domes with various topologies and dimensions in plan by Babaei and Sheidaei (2013). An investigation on the characteristics and feasibility of different tension schemes and also checking the accuracy of the numerical model and its calculated results is performed for suspended dome by Nie *et al*. (2013). In Kamyab and Salajegheh (2014), an enhanced particle swarm optimization (EPSO) algorithm is presented for size optimization of nonlinear scallop domes subjected to static loading. A genetic simulated annealing algorithm (GASA) is utilized to perform, partial and overall optimizations for a single-

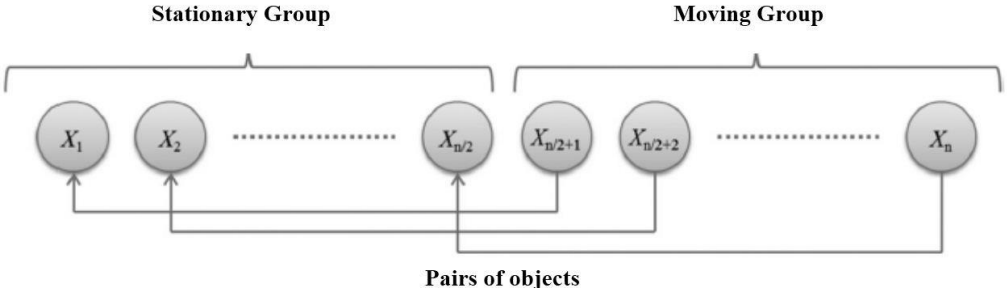

Fig. 2 Colliding body groups and the pairs of objects for collision

Table 1 The standard cable sections according to BS 5896

Diameter (mm)	Tensile strength (MPa)	Mass (g/m)	Cross sectional area (mm^2)	Yield stress at 0.1 % elongation
8	1860	296.8	38.0	60.8
9.3	1860	406.1	52.0	83.2
9.6	1960	429.6	55.0	87.7
11.3	1860	585.8	75.0	120.0
12.5	1860	726.3	93.0	149.0
12.9	1860	781.0	100.0	160.0
15.2	1770	1093.0	139.0	212.0
15.7	1770	1172.0	150.0	240.0

layer spherical shell that collapses due to instability under earthquake action by Wenzhheng and Jihong (2014). The topology and geometry optimization of different types of domes are investigated using ECBO by Kaveh and Rezaei (2015).

In Chen *et al.* (2015), the relative stiffness of the upper structure and the support stiffness is conducted, and the key parameter influencing the structural behavior is obtained. The steel roof of bicycle gymnasium in Tianjin Sports Center adopts suspended dome, in which the double-layer lattice shell is employed for the dome with the span 126 m×100 m and the height of 18 m (Wang 2015). The elliptic parabolic suspended dome for roof is adopted by Qing yang Gymnasium with span of span is 99.521 m×70.693 m (Yan 2015), Fig. 2.

Recently, Sadollah *et al.* (2015) developed Water Cycle, Mine Blast and improved mine blast algorithms, Gonçalves *et al*. (2015) presented Search Group Algorithm, and Mirjalili developed the Ant Lion Optimizer (2015). The rest of this paper is organized as follows. Section 2 consists of optimum design of dome structures according to LRFD domes. Section 3 recalls the laws of collision between two bodies. Topology and geometry optimization of single layer pin-jointed lamella dome is investigated in Section 4. Comparative study is performed between optimal design of dome with pin-joint and rigid-joint connections using ECBO algorithm in Section 5. Finally, Section 6 summarizes the main findings of this study.

2. Optimum design problem of suspended domes according to LRFD

Optimal design of domes consists of finding optimal sections for elements, optimal height for

Table 2 The allowable steel pipe sections taken from LRFD AISC

	Type	Nominal diameter (in)	Weight per ft (lb)	Area (in^2)	I (in^4)	S (in^3)	J (in^4)	Z (in^3)
1	ST	½	0.85	0.250	0.017	0.041	0.082	0.059
2	EST	½	1.09	0.320	0.020	0.048	0.096	0.072
3	ST	¾	1.13	0.333	0.037	0.071	0.142	0.100
4	EST	¾	1.47	0.433	0.045	0.085	0.170	0.125
5	ST	1	1.68	0.494	0.087	0.133	0.266	0.187
6	EST	1	2.17	0.639	0.106	0.161	0.322	0.233
7	ST	1 ¼	2.27	0.669	0.195	0.235	0.470	0.324
8	ST	1 ½	2.72	0.799	0.310	0.326	0.652	0.448
9	EST	1 ¼	3.00	0.881	0.242	0.291	0.582	0.414
10	EST	1 ½	3.63	1.07	0.666	0.561	1.122	0.761
11	ST	2	3.65	1.07	0.391	0.412	0.824	0.581
12	EST	2	5.02	1.48	0.868	0.731	1.462	1.02
13	ST	2 ½	5.79	1.70	1.53	1.06	2.12	1.45
14	ST	3	7.58	2.23	3.02	1.72	3.44	2.33
15	EST	2 ½	7.66	2.25	1.92	1.34	2.68	1.87
16	DEST	2	9.03	2.66	1.31	1.10	2.2	1.67
17	ST	3 ½	9.11	2.68	4.79	2.39	4.78	3.22
18	EST	3	10.25	3.02	3.89	2.23	4.46	3.08
19	ST	4	10.79	3.17	7.23	3.21	6.42	4.31
20	EST	3 ½	12.50	3.68	6.28	3.14	6.28	4.32
21	DEST	2 ½	13.69	4.03	2.87	2.00	4.00	3.04
22	ST	5	14.62	4.30	15.2	5.45	10.9	7.27
23	EST	4	14.98	4.41	9.61	4.27	8.54	5.85
24	DEST	3	18.58	5.47	5.99	3.42	6.84	5.12
25	ST	6	18.97	5.58	28.1	8.50	17.0	11.2
26	EST	5	20.78	6.11	20.7	7.43	14.86	10.1
27	DEST	4	27.54	8.10	15.3	6.79	13.58	9.97
28	ST	8	28.55	8.40	72.5	16.8	33.6	22.2
29	EST	6	28.57	8.40	40.5	12.2	24.4	16.6
30	DEST	5	38.59	11.3	33.6	12.1	24.2	17.5
31	ST	10	40.48	11.9	161	29.9	59.8	39.4
32	EST	8	43.39	12.8	106	24.5	49.0	33.0
33	ST	12	49.56	14.6	279	43.8	87.6	57.4
34	DEST	6	53.16	15.6	66.3	20.0	40.0	28.9
35	EST	10	54.74	16.1	212	39.4	78.8	52.6
36	EST	12	65.42	19.2	362	56.7	113.4	75.1
37	DEST	8	72.42	21.3	162	37.6	75.2	52.8

the crown, optimal number of the joints in each ring and the optimum number of rings, under the determined loading conditions. The allowable and standard cables which should be used in tensegrity system (hoop and radial cable) are shown in Table 1, also the allowable cross sections of steel elements are 37 steel pipe sections as shown in Table 2, which are standard sections. In this

table the abbreviations ST, EST, and DEST stand for standard weight, extra strong, and double-extra strong, respectively. These sections are taken from LRFD-AISC (1989) which is also utilized as the code of practice. The process of the optimum design of the dome structures includes introducing variables and constraints, and can be expressed as

$$\begin{aligned} &\text{Find} \quad \text{X}= \left[x_1, x_2, .., x_{ng}\right], h, Nr \\ &x_i \in \{d_1, d_2, \dots, d_{ng}\} \\ &h_i \in \{h_{min}, h_{min} + h^*, \dots, h_{max}\} \end{aligned} \tag{1}$$

To minimize

$$\text{V(x)} = \sum_{i=1}^{nm} x_i . l_i$$

Subjected to the following constraints:
Displacement constraint

$$\delta_i \leq \delta_i^{max} \qquad i = 1,2, \dots, nn. \tag{2}$$

Interaction formula constraints

$$\frac{P_u}{2\phi_c P_n} + \left(\frac{M_{ux}}{\phi_b M_{nx}} + \frac{M_{uy}}{\phi_b M_{ny}}\right) \leq 1 \quad for \frac{P_u}{\phi_c P_n} < 0.2 \tag{3}$$

$$\frac{P_u}{\phi_c P_n} + \frac{8}{9}\left(\frac{M_{ux}}{\phi_b M_{nx}} + \frac{M_{uy}}{\phi_b M_{ny}}\right) \leq 1 \quad for \frac{P_u}{\phi_c P_n} \geq 0.2 \tag{4}$$

where X is the vector containing the design variables of the elements; h is the variable of the crown height; Nr is the total number of rings; d_j is the jth allowable discrete value for the design variables, h_{min}, h_{max} and h^* are the permitted minimum, maximum and increased amounts of the crown height which in this paper are taken as $D/20$, $D/2$ and 0.25 m, respectively where D is the diameter of the dome; ng is the number of design variables or the number of groups; $V(x)$ is the volume of the structure; L_i is the length of membe i; δ_i is the displacement of node i; δ_{imax} is the permitted displacement for the ith node; nn is the total number of nodes; ϕ_c is the resistance factor (ϕ_c = 0.9 for tension, ϕ_c =0.85 for compression); ϕ_b is the flexural resistance reduction factor (ϕ_b = 0.9); M_{ux} and M_{uy} are the required flexural strengths in the x and y directions, respectively; M_{nx} and M_{ny} are the nominal flexural strengths in the x and y directions, respectively; P_u is the required strength; and P_n denotes the nominal axial strength which is computed as

$$P_n = A_g F_{cr} \tag{5}$$

where A_g is the gross area of a member; and F_{cr} is calculated as follows

$$F_{cr} = \left(0.658^{\lambda_c{}^2}\right).f_y \quad for\ \lambda_c \leq 1.5 \tag{6}$$

$$F_{cr} = \left(\frac{0.877}{\lambda_c^2}\right).f_y \quad for\ \lambda_c > 1.5 \tag{7}$$

Here, f_y is the specified yield stress; and λ_C is obtained from

$$\lambda_c = \frac{kl}{\pi r}\sqrt{\frac{f_y}{E}} \tag{8}$$

where k is the effective length factor taken as 1; l is the length of a dome member; r is governing radius of gyration about the axis of buckling; and E is the modulus of elasticity. In Eq. (9), V_u *is* the factored service load shear, V_n is the nominal strength in shear, and φ_v represents the resistance factor for shear (φ_v = 0.9).

$$V_u \leq \varphi_v V_n \tag{9}$$

2.1 Nominal strengths

Based on LRFD-AISC (1989) specification, the nominal tensile strength of a member is equal to

$$P_n = F_y A_g \tag{10}$$

where A_g is the gross section of the member.

The nominal compressive strength of a member is the smallest value obtained from the limit states of flexural buckling, torsional buckling, and flexural-torsional buckling. For members with compact and/or non-compact elements, the nominal compressive strength of the member for the limit state of flexural buckling is as follows

$$P_n = F_{cr} A_g \tag{11}$$

where F_{cr} is the critical stress based on flexural buckling of the member, calculated by Eq. (6) and Eq. (7).

In the above equations, l is the laterally unbraced length of the member; K is the effective length factor; r is the governing radius of gyration about the axis of buckling, and E is the modulus of elasticity.

3. Optimization algorithms

This section introduces the enhanced colliding bodies optimization algorithm. First, a brief description of standard CBO based on the work of Kaveh and Mahdavi (2015a, b) is provided, and then the ECBO is introduced, Kaveh and Ilchi Ghazaan (2014). Detailed explanation of these methods and recently developed metaheuristic algorithms can also be found in Kaveh (2014).

3.1 Colliding bodies optimization

The collision is a natural occurrence and the Colliding Bodies Optimization (CBO) algorithm was developed based on this phenomenon. In this method, one object collides with other object and they move towards a minimum energy level, Fig. 3. The CBO is simple in concept, does not depend on any internal parameters, and does not use memory for saving the best-so-far solutions. CBO algorithm, like other multi-agent methods, is a population-based meta-heuristic algorithm. Each solution candidate X_i containing a number of variables (i.e., X_i=$\{x_{i,j}\}$) is considered as a colliding body (CB). The massed objects composed of two main groups equally; namely stationary and moving objects, where moving objects collide to stationary objects to improve their positions and push stationary objects towards better positions. After the collision, the new position of colliding bodies are updated based on the new velocity by using the collision laws; and the lighter

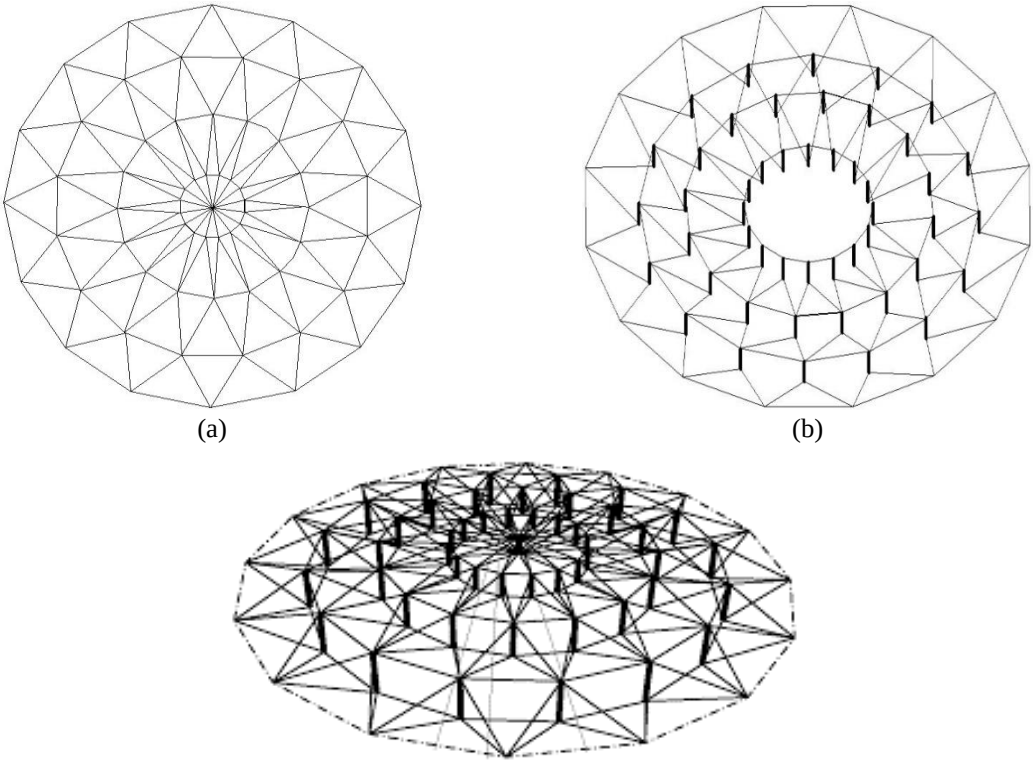

(a) (b)

(c)

Fig. 3 Basic arrangement of the suspended dome system. (a) Topmost lamella dome, (b) Tensegrity system, (c) Lamella suspended dome

and heavier CBs moves sharply and slowly, respectively.

The pseudo-code for the CBO algorithm can be summarize as follows:

Step 1: Initialization. The initial positions of CBs are determined with random initialization of a population of individuals in the search space

$$x_i^0 = x_{min} + rand(x_{max} - x_{min}), \quad i = 1,2,3,\dots,n \tag{12}$$

where x_i^0 determines the initial design vector of the *i*th CBs. x_{max} and x_{min} are the minimum and the maximum allowable values vector for the variables; *rand* is a random number in the interval [0, 1]; and *n* is the number of CBs.

Step 2: The magnitude of the body mass for each CB is defined as

$$m_k = \frac{\frac{1}{fit(k)}}{\sum_{i=1}^{n}\frac{1}{fit(i)}}, \quad k = 1,2,\dots,n \tag{13}$$

where $fit\ (i)$ represents the fitness value of the agent *i*; *n* is the population size. It is clear that a CB with a good value exerts a larger mass than the bad one. In maximization problems, the term (1/*fit*) is replaced by fit (i).

Step 3: Mating of bodies.

CBs costs are sorted in ascending order based on the value of cost function. The sorted CBs are divided equally into two groups:

• The lower half of CBs (stationary CBs) includes good agents that are stationary and velocity of these bodies before collision is zero. Thus

$$v_i = 0, \;\; i = 1, \dots, \frac{n}{2} \tag{14}$$

• The upper half of (moving CBs) includes agents that move toward the lower half. Then, the better and worse CBs, i.e., agents with upper fitness value, of each group will collided together. The change of the body position represents the velocity of this bodies before collision as

$$v_i = x_{i-\frac{n}{2}} - x_i, \quad i = \frac{n}{2} + 1, \dots, n \tag{15}$$

where v_i and x_i are the velocity and position vector of the *i*th CB in this group, respectively; $x_{i\text{-}n/2}$ is the *i*th CB pair position of x_i in the previous group.

Step 4: Updating velocities. After the collision, the velocity of bodies in each group is evaluated using Eqs. (16) and (17). The velocity of each moving CBs after the collision is defined by

$$v_i' = \frac{\left(m_i - \varepsilon m_{i-\frac{n}{2}}\right) v_i}{m_i + m_{i-\frac{n}{2}}} \qquad i = \frac{n}{2} + 1, \frac{n}{2} + 2, \dots, n \tag{16}$$

where v and v_i^0 are the velocity of the *i*th moving CB before and after the collision, respectively; m_i is mass of the *i*th CB; $m_{i\text{-}n/2}$ is mass of the *i*th CB pair. Also, the velocity of each stationary CB after the collision is specified by

$$v_i' = \frac{\left(m_{i+\frac{n}{2}} + \varepsilon m_{i-\frac{n}{2}}\right) v_{i+\frac{n}{2}}}{m_i + m_{i+\frac{n}{2}}} \qquad i = 1,2, \dots, \frac{n}{2} \tag{17}$$

where $v_{i+\frac{n}{2}}$ and v_i^0 are the velocity of the *i*th moving CB pair before the collision and the *i*th stationary CB after the collision, respectively; m_i is mass of the *i*th CB; $m_{i+\frac{n}{2}}$ is the mass of the *i*th moving CB pair; ε is the coefficient of restitution (COR), which is defined as the ratio of the separation velocity of two agents after collision to the approach velocity of two agents before collision. For most of the real objects, ε is between 0 and 1, which after collision the separation velocity of bodies is low and high, respectively. Therefore, to control exploration and exploitation rate, COR decreases linearly from unity to zero.

Thus, it is stated as

$$\varepsilon = 1 - \frac{iter}{iter_{max}} \tag{18}$$

Step 5: Updating positions.

New positions of CBs are evaluated using the generated velocities after the collision in position of stationary CBs. The new positions of each moving CB is calculated by

$$x_i^{new} = x_{i-\frac{n}{2}} + rand\ o\ v_i', \quad i = \frac{n}{2} + 1, \dots, n \tag{19}$$

where $x_i^{new\prime}$ and v_i' are the new position and the velocity after the collision of the *i*th moving CB, respectively; $x_{i-n/2}$ is the old position of *i*th stationary CB pair. Also, the new position of each stationary CB is

$$x_i^{new} = x_i + rand\ o\ v_i', \quad i = 1,2, \dots, \frac{n}{2} \tag{20}$$

where x_i^{new} ; x_i and v_i^0 are the new position, old position and the velocity after the collision of the *i*th stationary CB, respectively. *Rand* is a random vector uniformly distributed in the Range [-1,1] and the sign ''o'' denotes an element-by-element multiplication.

Step 6: Terminating criterion.

The process of optimization is terminated when the maximum number of analyses is attained. For further details, the reader may refer to Kaveh and Mahdavi (2015b).

3.2 Enhanced colliding bodies optimization

A modified version of the CBO is Enhanced Colliding Bodies Optimization, which improves the CBO to get faster and more reliable solutions. The introduction of memory increases the convergence speed of ECBO compared to the standard CBO. Furthermore, changing some components of colliding bodies will help ECBO to escape from local optima. The steps of the ECBO are as follows:

Step 1: Initialization

The initial positions of all CBs are determined randomly in an m-dimensional search space according to Eq. (10). Where x_i^0 is the initial solution vector of the *i*th CB. Here, x_{min} and x_{max} are the bounds of design variables; random is a random vector which each component is in the interval [0, 1]; *n* is the number of CBs.

Step 2: Defining mass

The value of mass for each CB is evaluated according to Eq. (13).

Step 3: Saving

Considering a memory which saves some historically best CB vectors and their related mass and objective function values can make the algorithm performance better without increasing the computational cost, Kaveh and Ghazaan (2014). Here a Colliding Memory (CM) is utilized to save a number of the best-so-far solutions. Therefore in this step, the solution vectors saved in CM are added to the population, and the same numbers of current worst CBs are deleted. Finally, CBs are sorted according to their masses in a decreasing order.

Step 4: Creating groups

CBs are divided into two equal groups: (i) stationary group and (ii) moving group. The pairs of CBs are shown in Fig. 3.

Step 5: Criteria before the collision

The velocity of stationary bodies before collision is zero (Eq. (14)). Moving objects move toward stationary objects and their velocities before collision are calculated by Eq. (15).

Step 6: Criteria after the collision

The velocities of stationary and moving bodies are evaluated using Eqs. (16) and (17), respectively.

Step 7: Updating CBs

The new position of each CB is calculated by Eqs. (18) and (19).

Step 8: Escape from local optima

Meta-heuristic algorithms should have the ability to escape from the trap when agents get close to a local optimum. In ECBO, a parameter like *Pro* within (0, 1) is introduced and it is specified whether a component of each CB must be changed or not. For each colliding body *Pro* is compared with rn_i (i =1, 2… n) which is a random number uniformly distributed within (0, 1). If rn_i < *Pro*, one dimension of the *i*th CB is selected randomly and its value is regenerated as follows

$$x_{ij} = x_{j,min} + random.\left(x_{j,max} - x_{j,min}\right) \tag{21}$$

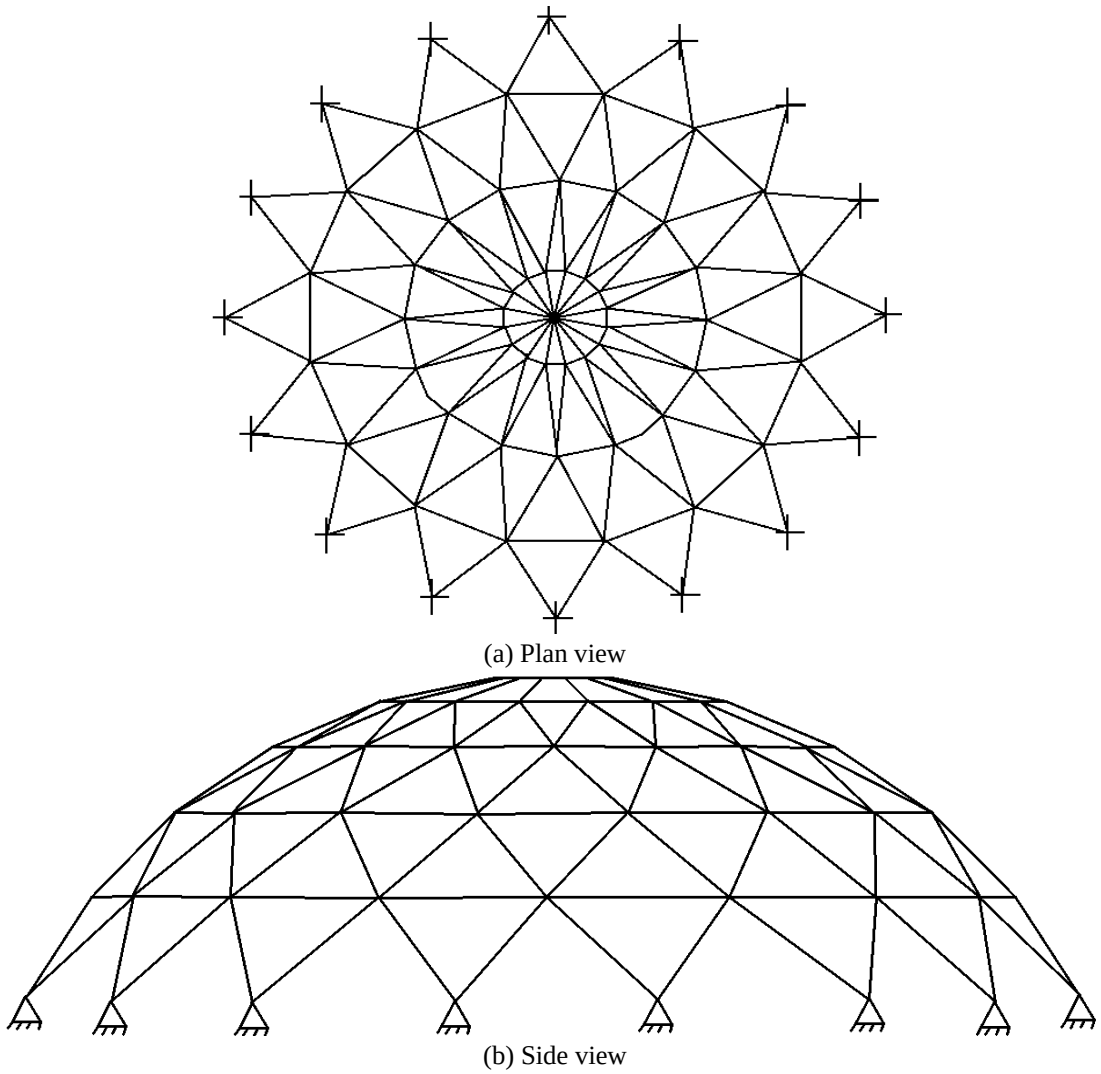

(a) Plan view

(b) Side view

Fig. 4 Schematic of a lamella dome. (a) Joint coordinates of a single layer lamella dome, (b) side view coordinate

where x_{ij} is the *j*th variable of the *i*th CB. $x_{j,min}\ and\ x_{j,max}$, are the lower and upper bounds of the *j*th variable respectively. In order to protect the structures of CBs, only one dimension is changed. This mechanism provides opportunities for the CBs to move all over the search space thus providing better diversity.

Step 9: Terminating condition check

The optimization process is terminated after a fixed number of iterations. If this criterion is not satisfied go to Step 2 for a new round of iteration.

4. Configuration of single layer lamella dome and suspended dome

4.1 Configuration of lamella domes shell

Topology of a single layer lamella dome are shown in Fig. 4. Similar to all other domes, for lamella dome it is possible to generate the structural data for the geometry if three parameters consisting of the diameter (*D*) of the dome, the total number of rings, and the height of the crown (*h*) are known. When the geometry of a dome is formed according to the mentioned parameters, the topology of domes can be obtained. The topology contains the total number of members, member incidences, total number of joints, and joint coordinates of the domes. The distances between the rings in the dome on the meridian line are generally made to be equal. It can be easily seen from Figs. 5(a) and 5(b) that all the joints are located with equal distance between each other on the same ring in both domes. The top joint, known as the crown, is numbered as the first joint (joint number 1). The first joint on the first ring is numbered as joint 2 in any dome type. In lamella dome there are the same number of joints on each ring. The joint numbers of all the other first joints of the other rings are computed from the following equation

$$J_{r1} + (r - 1) \times 10 \tag{22}$$

where r is the ring number, and J_{r1} is the first joint number of the first ring namely 2 for lamella dome. It worthwhile to mention that all of the first joints of the odd numbered rings (ring 1 and ring 3) are located on the radius that makes angle of 16° with the *x*-axis and similarly, the first joints of the evenly numbered ring 2 is located on the intersection points of that ring and the *x*-axis in lamella dome. First member is taken as the one connecting joint 1 to joint 2 which makes angle of (360/*Nn*)° with *x*-axis in lamella dome. For the first ring group, the start node for all elements is the joint number 1 and the end nodes are those on the first ring. The start and end nodes of ring elements can be obtained using Eqs. (24) and (25), and for other rings 2 and 3, this process is repeated and all the member incidences are similar.

$$\begin{cases} x_i = \dfrac{D}{2Nr}\cos\left(\dfrac{360}{4n_i}\left(i - \displaystyle\sum_{j=1}^{i-1} 4n_j - 1\right)\right) \\ z_i = \sqrt{\left(R^2 - \dfrac{n_i^2 D^2}{4Nr^2}\right)} - (R - h) \\ y_i = \dfrac{D}{2Nr}\sin\left(\dfrac{360}{4n_i}\left(i - \displaystyle\sum_{j=1}^{i-1} 4n_j - 1\right)\right) \end{cases} \tag{23}$$

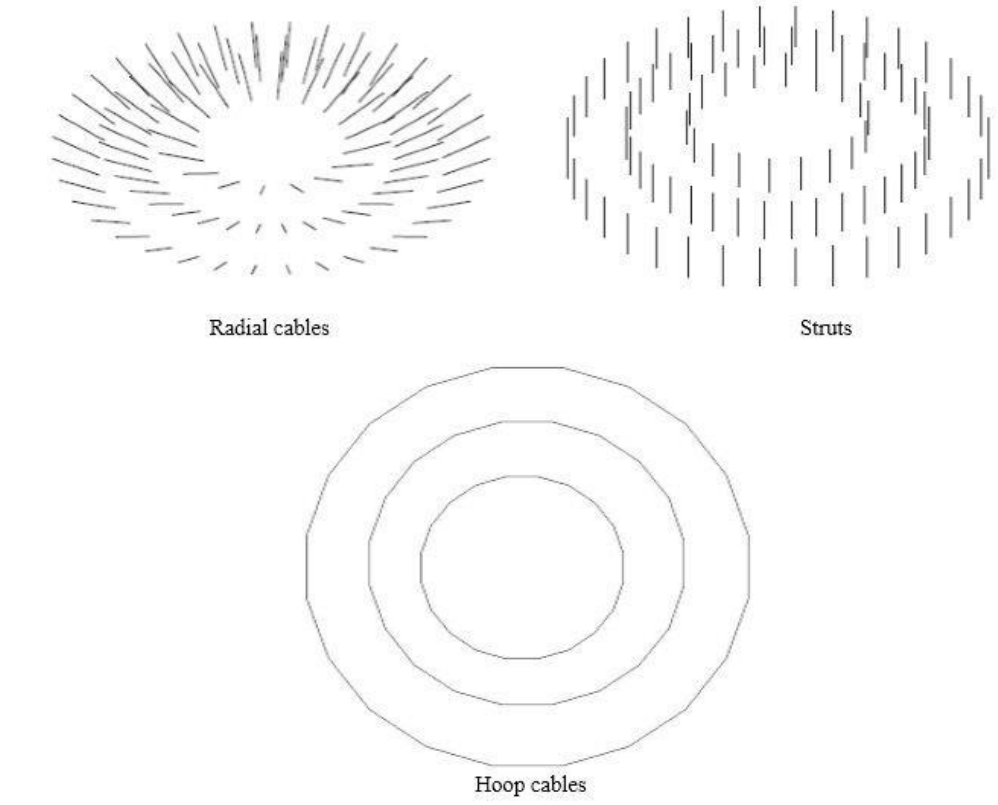

(a)

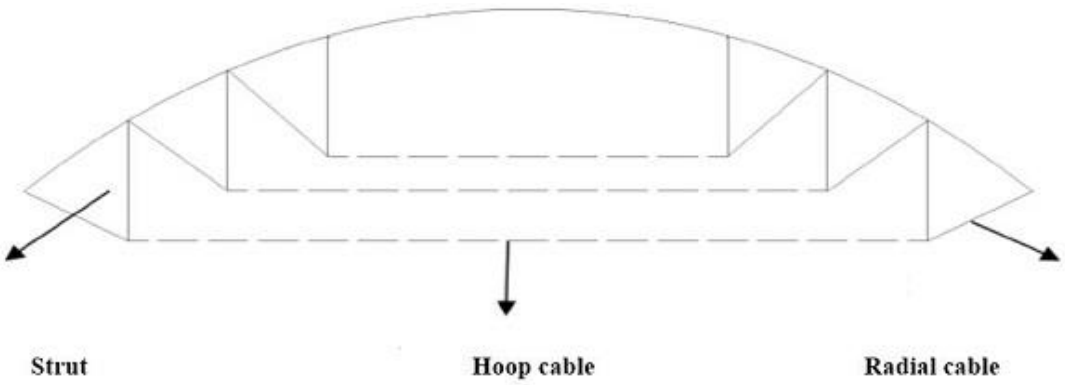

(b)

Fig. 5 Configuration of tensegrity system of suspended dome. (a) and (b)

$$\begin{cases} I = 10 * (n_i - 1) + J + 1 \\ J = 10 * (n_i - 1) + J + 2 \end{cases} \quad \begin{pmatrix} j=1,2,3,\dots,9 \\ n_i=1,2,\dots,Nr-1 \end{pmatrix} \tag{24}$$

$$\begin{cases} I = 10 * (n_i - 1) + 2 \\ J = 10 * n_i + 1 \end{cases} \quad n_i = 1,2,\dots,Nr-1 \tag{25}$$

Computation of *x*, *y*, and *z* coordinates of a joint on the domes requires the angle between the line that connects the considered joint to joint placed at the crown of dome (joint number 1) and the *x*-axis as shown in Fig. 5. For lamella dome, for the odd numbered rings the mentioned angle can be computed by Eqs. (26) and (27) for the odd and even numbered rings, respectively.

$$a_i = \frac{360}{2 * Nn} \tag{26}$$

$$a_i = \frac{360}{2 * Nn} \left(i - j_{r,1}\right) \tag{27}$$

r is the ring number that joint *i* is placed on it and *j* is the first joint number on the ring number *r* which is on the *x*-axis. The members group which is used in Tables is mentioned in the following sentences. For lamella domes, the ribbed members between the crown and the first ring are group 1, the diagonal members between fist ring and second ring are group 2, the diagonal members between second ring and third ring are group 3. The members on the first ring are group 4, and the members on the second ring are group 5.

4.2 Configuration of lamella suspended domes

The lower tensegric system is detached from the upper single layer dome as an independent system. In the lower tensegric system, the cables and the vertical struts are hinged in the joints. The tensegrity system is constructed of four rings of hoop steel cables, radial steel cables and struts at the lower part of model. The cables are tension-only elements and the vertical struts are also compression elements.

The topmost single layer lamella dome is arranged as a triangle circular truss. The struts which are the web members of suspended dome and bending members which are the elements of single layer lamella dome, which are circular standard steel tubes, the sections which are listed in Table 1.

As it mentioned before, the suspended dome is constructed by combining tensegrity system (cable-strut) and single layer reticulated dome. The configuration of single layer lamella dome is explained in the previous section. As it can be seen from Fig. 6, the tensegrity system is constructed of hoop cable, radial cable and compression struts. The topology of tension only cable which are called radial and hoop cables are the same as the upper single layer reticulated dome. Therefore, the suitable configuration of tensegrity system depends on its upper single layer dome.

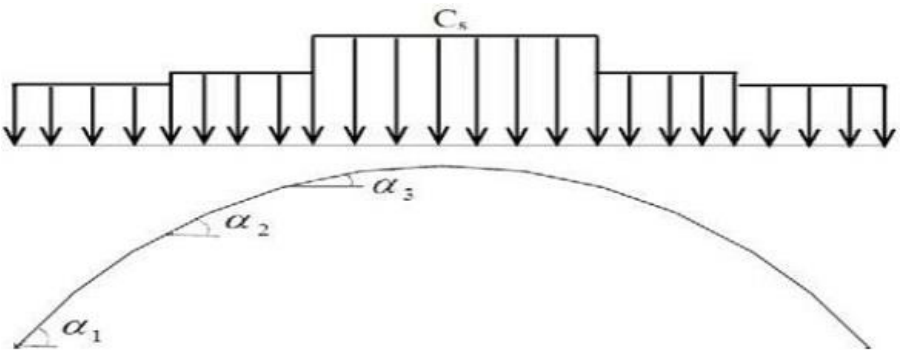

Fig. 6 The coefficients C_s for distribution on a dome roof

The suspended dome which is discussed in this study use the configuration of lamella dome as upper part. Therefore the configuration of tensegrity system should be obtained inspiring the configuration of lamella dome. The current tensegrity system connect to rings 3, 4 and 5 of single layer lamella dome by vertical struts elements.

Computation of *x* and *y* coordinates of a joint on tensegrity system requires the angle between the line that connects the considered joint to joint placed at the crown of dome (joint number 1) and the *x*-axis. For lamella suspended dome, for the odd numbered rings the mentioned angle can be computed by Eqs. (26) and (27) for the odd and even numbered rings, respectively.

Computation of *z* coordinates of a joint on tensegrity system can be obtained using the following equation

$$z_i = \sqrt{\left(R^2 - \frac{n_i^2 D^2}{4Nr^2}\right)} - (R - h) - Hhoop(i) \tag{28}$$

where, *Hhoop* is the length of strut, which is the distance between the topmost layer and the tensegrity system. Also, n_i is the number of ring corresponding to the joint *i* of topmost shell and *R* is the radius of the hemisphere.

For lamella suspended dome, the diagonal members between the crown and the first ring are group 1, the diagonal members between second ring and third ring are group 2, the diagonal members between second ring and third ring are group 3, the first ring, second ring and third ring are group 4, 5 and 6, respectively. Then, after third ring each diagonal member and its related ring are numbered respectively. For example, group 7 is diagonal member between the ring 3 and 4, then the group 8 is the fourth ring of the dome.

5. Design loads

According to ASCE 7-05 there are some specific considerations for loading conditions of arched roofs such as dome structures. In this study, the load conditions are taken from Kaveh *et al*. (2013).

5.1 Dead load

The design dead load is established on the basis of the actual loads that may be expected to act on the structure of constant magnitude. The weight of various accessories, cladding, supported lighting, heat and ventilation equipment, and the weight of space frame comprise the total dead load. In this study, a uniform dead load of 200 kg/m^2 is considered for estimated weight of the sheeting, space frame, and nodes of the dome structures.

5.2 Snow load

The snow load for arched roofs is calculated according to mentioned codes. Snow loads acting on a sloping surface is assumed to act on the horizontal projection of that surface, Fig. 7. The snow load (*Ps*) should be obtained by multiplying the flat roof snow load (P_f) by the roof slope factor (C_s) as follows

$$P_s = C_s . P_f \tag{29}$$

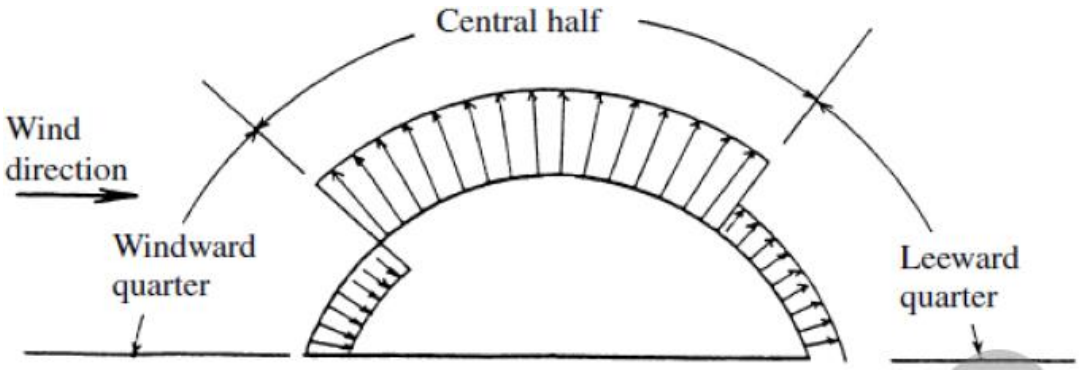

Fig. 7 Side view of a dome roof under wind pressure

where depending on the slop of the roof, C_s is

$$C_s = \begin{cases} 1.0 & \alpha < 15^\circ \\ 1.0 - \frac{\alpha - 15^\circ}{60^\circ} & 15^\circ < \alpha < 60^\circ \\ 0.25 & \alpha > 60^\circ \end{cases} \tag{30}$$

5.3 The design procedure under wind load according to ASCE 7-05

The design procedure can be explained as follow:

Step 1. The basic wind speed (V) and wind directionality factor (K_d) for arched roofs, can be determined in accordance with Section 6.5.4 of ASCE 7-05. The basic wind speed V, used in the determination of design wind loads on buildings and other structures is as given in Fig. 6-1 of ASCE 7-05. Basic Wind Speed V and Wind Directionality Factor K_d are taken from ASCE 7-05 as 40m/s and 0.85, respectively.

Step 2. An importance factor, I, for the domes or other structure is determined from Table 6-1 of ASCE 7-05 which can be considered as 1.15 for domes.

Step 3. An exposure category is determined for each wind direction in accordance with Section 6.5.6. The exposure category is assumed as C according to situation which is defined in part 6.5.6 of ASCE 7-05, and K_z can be determined from the following formula

$$K_z = 2.01 * (\frac{15}{Z_g})^{2/\alpha} \tag{31}$$

Step 4. A topographic factor (K_{zt}) is determined in accordance with Section 6.5.7 of ASCE 7-05. It is assumed as 1 in this study.

Step 5. A gust effect factor (G_f) is determined in accordance with Section 6.5.8 of ASCE. For rigid structures the gust-effect factor is taken as 0.85.

Step 6. An enclosure classification is determined in accordance with Section 6.5.9 of ASCE 7-05. It is assumed to be enclosed, since all lateral and upper parts of the domes are closed and subjected to wind pressure directly.

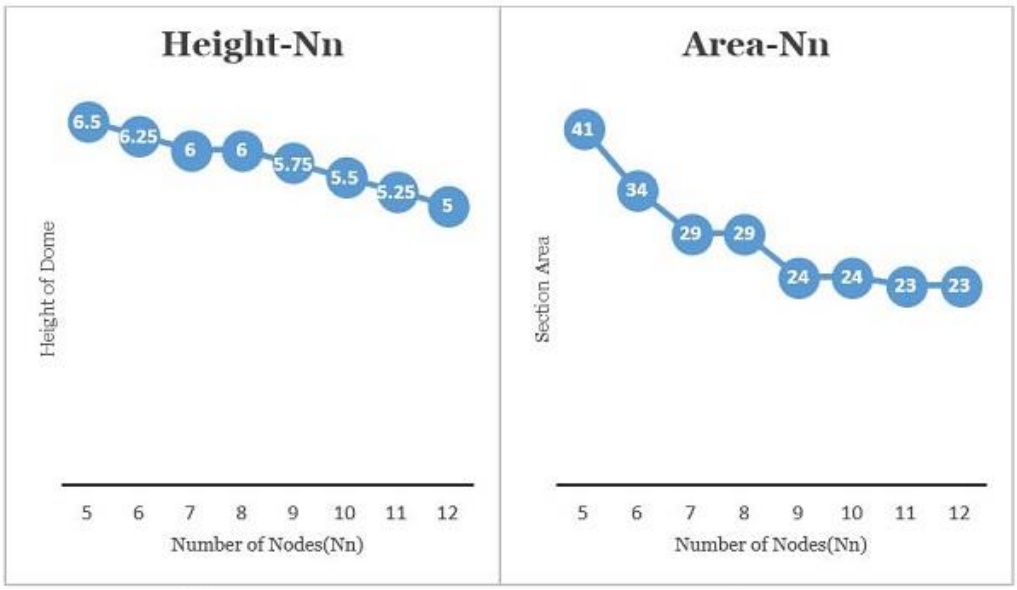

(a) (b)

Fig. 8 (a) Number of nodes in each ring and its effect on average section area (b) Number of nodes in each ring and its effect on height of dome

Step 7. Velocity pressure, q_z, should be calculated by the following equation

$$q_z = 0.613\, K_z\, K_{zt}\, K_d\, V^2\, I \tag{32}$$

Step 8. Internal pressure coefficient GCpi is determined in accordance with Section 6.5.11.1 of ASCE 7-05. These are considered +0.18 and –0.18 for enclosed structures from Figs. 6-5 of ASCE 7-05. Plus and minus signs signify pressures acting towards and away from the internal surfaces, respectively.

Step 9. External pressure coefficients *Cp* is determined in accordance with Section 6.5.11.2. *Cp* is found from Figs. 6-7 which is for domes in ASCE 7-05 which is adopted from Eurocode 1995. The dome is assumed to be separated into three parts as shown in Fig. 8, such as windward part, center part and leeward part. Three different external pressure coefficients for these three parts of the dome are calculated with respect to rise-to-span ratio (*r*) and *Cp* is determined from a graph, which is depicted in Figs. 6-7 of ASCE 7-05.

Step 10. Design wind pressure is calculated from Eq. (36) of ASCE 7-05

$$p = qG_f C_p - q\left(GC_{pi}\right) \tag{33}$$

6. Results and discussion

In this section, the dome described in the previous section is optimized utilizing the ECBO. The modulus of elasticity for the steel is taken as 205 kN/mm^2. The limitations imposed on the joint displacements are 28 mm in the *z* direction and 33 mm in the *x* and *y* directions for the 1st, 2nd and 3rd nodes, respectively, Table 3.

Table 3 Displacement restrictions of single layer ribbed and Schwedler domes

Joint No.	Displacement limitations (mm)					
	X-direction		*Y*-direction		*Z*-direction	
	Upper bound	Lower bound	Upper bound	Lower bound	Upper bound	Lower bound
1	–	–	–	–	28	−28
2	33	−33	33	−33	28	−28
3	33	−33	33	−33	28	−28

The behavior of domes is nonlinear due to the change of geometry under external loads, therefore nonlinear analysis is performed in this study. This is due to the imperfections arising either from the manufacturing process and/or from the construction of the structure. Furthermore domes are sometimes subjected to equipment loading concentrated at the crown in addition to uniform gravity load. In the further step of this study, the domes are also subjected to equipment loading.

Another significant criterion governing the design of domes is the requirement of full triangulation of the geometry. Also this is one of the reasons for choosing lamella dome. Since these types of structures have a high stiffness in all directions and are kinematically stable, triangulation must be used in the design of domes unless making rigid connection designs. Therefore, for pin-connected dome design, the latticed shell must be formed from the triangular units, otherwise stability

6.1 Optimum topology design of single layer dome with pin-joint connections using the ECBO

The LRFD specification and drift limitation are considered as the constraints for this structure. The modulus of elasticity for the steel is taken as 205 kN/mm^2. The diameter of the dome is selected as 20 m. The limitations imposed on the joint displacements are according to Table 3. The volume of the dome structures can be considered as a function of the average cross-sectional area of the elements ($\bar{A}$) and the sum of the element lengths, expressed as

$$\mathbf{V}(X) = \overline{A} \; . \; \sum_{i=1}^{nm} L_i \tag{34}$$

6.1.1 Effects of Nn on the optimum design

In this part the number of nodes in each ring (*Nn*), the height of dome and area section of elements are defined as the design variables in our formulation. The optimum values for these variables can directly be obtained. However, in order to investigate the effect of *Nn* on the optimum designs, here we consider all possible conditions for these design variables. The dome is considered to be subjected to the vertical downward load of -500 kN and two horizontal loads of 150 kN in the x and y directions at its crown.

Table 4 lists the optimal designs for the lamella dome with different *Nn* obtained by the ECBO algorithm when *Nr* is equal to 3. From this table it can be observed that a dome with small number of elements (*Nn*) tends to select a greater height. When *Nn* increases, the height of the dome decreases, Fig. 9(a). For a dome with small *Nn*, having a large height helps the dome to prevent instability. In addition, the selected sections for the elements in a dome with a small *Nn* are

Table 4 Geometry and topology optimization of pin-jointed lamella dome using enhanced colliding body optimization

Optimum design of the lamella dome with three rings								
Optimum sections (designations)								
Group number	Nn=5	Nn=6	Nn=7	Nn=8	Nn=9	Nn=10	Nn=11	Nn=12
1	PIPST (12)	PIPST (10)	PIPST (10)	PIPST (6)	PIPST (6)	PIPST (6)	PIPST (6)	PIPST (6)
2	PIPST (4)	PIPST (5)	PIPST(31/2)	PIPST (5)	PIPST(31/2)	PIPST(31/2)	PIPST (6)	PIPST (3)
3	PIPST (5)	PIPST (5)	PIPST (4)	PIPST (5)	PIPST(31/2)	PIPST(31/2)	PIPST (6)	PIPST(31/2)
4	PIPST (6)	PIPST (6)	PIPST (6)	PIPST (6)	PIPST (6)	PIPST (6)	PIPST (6)	PIPST (6)
5	PIPST (5)	PIPST (5)	PIPST(31/2)	PIPST (4)	PIPST(31/2)	PIPST(31/2)	PIPST (3)	PIPST (3)
Height (m)	6.50	6.25	6.00	6.00	5.75	5.50	5.25	5.00
Max.displacement (cm)	2.76	2.76	2.78	2.78	2.79	2.69	2.73	2.72
Max. strength ratio	78.94	50.78	80.55	62.56	75.39	61.85	94.22	86.20
Volume (m^3)	0.64	0.66	0.55	0.70	0.5572	0.5918	0.5904	0.62
L_i (m)	197.03	214.57	231.64	250.61	267.25	283.53	299.46	315.04
$\bar{A}$ (cm^2)	41.22	34.68	29.04	29.58	24.77	24.77	23.66	23.66

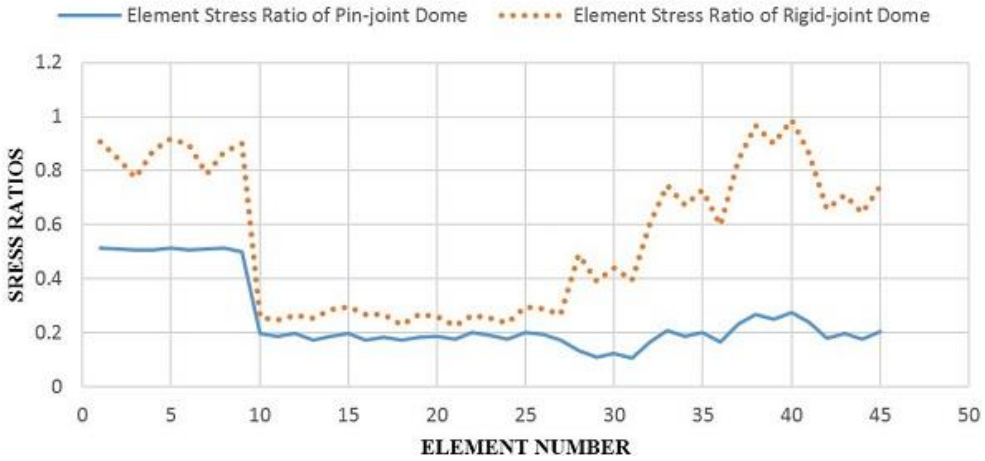

Fig. 9 Compression of the stress ratios of single layer lamella dome with pin-jointed and rigid-jointed connections

stronger than those of a dome with a large value for *Nn*, Fig. 9(b). This means that although a dome with small *Nn* has a small value for the sum of the element lengths, however its average cross sectional area is a big value. In short, the lowest weight design is the one which has the smallest values for the average cross sectional area and the sum of the element lengths, simultaneously.

Table 4 presents the results for the pin-jointed lamella dome. The optimum designs are obtained when *Nn* is set to 5, 6 and 7. For the smaller values of *Nn*, as it is expected, the sections are very strong and therefore the average cross sectional area becomes a higher value, and on the contrary for the big values of *Nn*, the sum of the element lengths increases the volume of the dome. The dominant constraints of the designs are often the displacement constraint; however

Table 5 The values of the joint displacements (m) for the optimum single layer pin-jointed lamella dome with *Nn*=9 and *Nr*=3

Direction		*X*-direction	*Y*-direction	*Z*-direction
Joint no	1	$+1.38\times10^{-3}$	$+1.38\times10^{-3}$	-2.79×10^{-2}
	2	$+3.11\times10^{-3}$	$+1.94\times10^{-3}$	-1.95×10^{-3}
	3	$+2.16\times10^{-3}$	$+3.03\times10^{-3}$	-1.84×10^{-4}

Table 6 Three parts of the lamella dome with three rings and their specifications

Total joints of the dome	28		
Total surface area of the dome	S_a (variable)		
Areas (3 part)	Forward quarter	Center quarter	Leeward quarter
Number of joints	6	16	6
Related area	$0.2*S_a$	$0.8*S_a$	$0.2*S_a$

changing a section of the reported designs to a lighter one often causes swerving the stress constraints in the elements. Firstly with a higher probability a small height will be a suitable choice rather than a big one for domes with high *Nn*. In other words, we expect when the value of the *Nn* increases, the height of the dome decreases. In addition, the value of $\bar{A}$ must be decreased as much as possible when *Nn* increases. Therefore, for the domes with small *Nn*, we will have stronger sections. These points are supported by the comparisons of the results made in Tables 4. The values of the joint displacements (m) for the optimum single layer pin-jointed lamella dome with *Nn*=9 and *Nr*=3 are shown in Table 5.

6.2 Optimum designs of single layer rigid-jointed and pin-jointed lamella dome using ECBO

The single layer lamella dome with rigid-joint and pin-joint connections are compared in this section. The diameter of the domes is selected as 20 m. To investigate the real performance of these domes, they are subjected to wind, dead, snow and vertical equipment loads. It is worthwhile to mention that the wind load is applied on domes according to the provision ASCE 7-05 which is illustrated in Section 5.3. The vertical downward load is equal to -500 kN and it is concentrated on its crown. The design dead load is established on the basis of the actual loads like the weight of cladding that may be expected to act on the dome structure. The dead and snow loads are considered as 200 N/m^2 and 800 N/m^2, respectively. Dead and snow loads are converted into equivalent point load for each joint for the sake of simplicity. For this conversion distributed load is multiplied by surface area of dome, Table 6. The projected area depends on the height of domes and it is calculated by Eq. (35), where *r* is the radius of the dome, and *h* is the height of the dome.

$$S_a = \pi(h^2 + r^2) \tag{35}$$

Considering the sign of internal pressure, two loading conditions for internal pressure can be present. Therefore, positive or negative internal pressure can be applied on domes. In this study we assume that the internal pressure is positive and then the downward internal pressure is applied on the dome which is the critical loading condition, because it has the same direction as the dead and snow loads.

Table 7 Optimum design of pin-jointed and rigid-jointed lamella dome obtained using the ECBO algorithm

		ECBO algorithm	
		Pin-jointed	Rigid-jointed
Optimum number of rings		3	3
Optimum tubular	Group 1	PIPST(6)	PIPST(5)
Section designations	Group2	PIPST(5)	PIPST(4)
	Group 3	PIPST(5)	PIPST(4)
	Group 4	PIPST(5)	PIPST(5)
	Group 5	PIPST(6)	PIPST(5)
Optimum height of crown (m)		6.00	6.25
Maximum displacement (cm)		2.71	2.77
$\sum l_I(m)$		269.78	272.58
$A(cm^2)$		31.04	24.82
Maximum strength ratio		51.88	87.66
Volume (m^3)		0.8076	0.6245

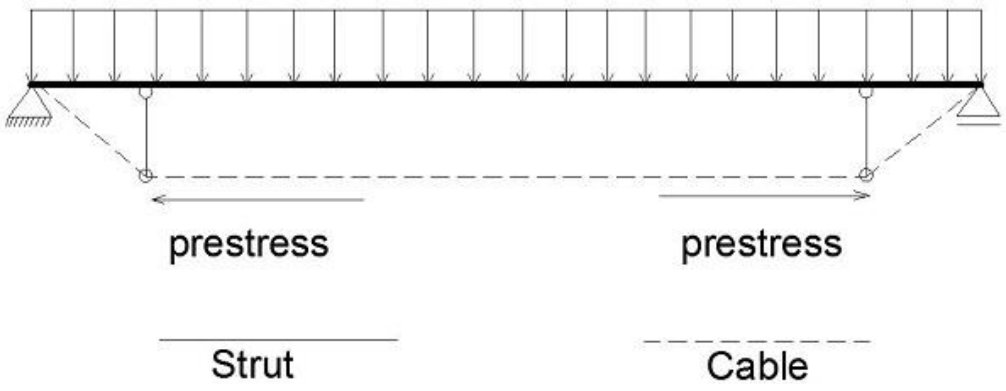

(a) Uniformly distributed load and cable pre-stressed force

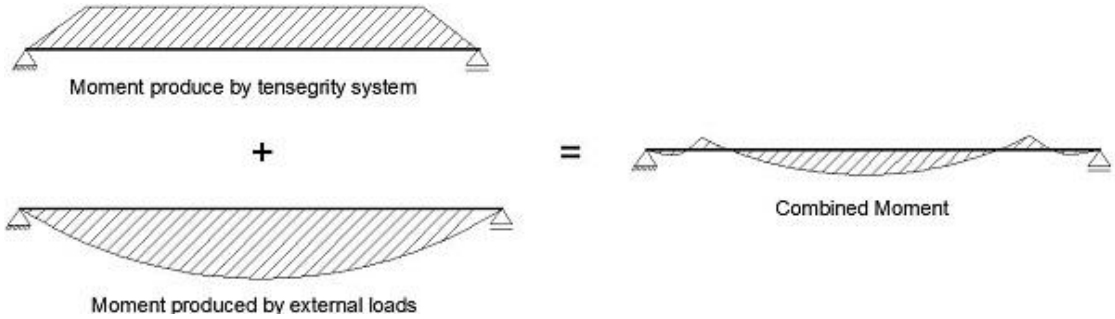

Fig. 10 Bending moment diagrams of a simply supported beam under tensegrity load and external load

According to the result of the previous section, the optimum number of the joints in each ring and the optimum number of rings are considered as 9 and 3, respectively, because with using these values the optimum volume of lamella dome with pin-joint connections will be obtained.

In this section, as it was mentioned, the dead, snow, equipment and wind loads are applied on lamella domes to investigate the real behavior of the dome, and also to obtain the optimum volume

of dome under these loading conditions.

Table 7 shows the optimum results of single layer lamella dome with pin-joint and rigid-joint connections. The results of this problem prove that domes with rigid connection must be used in case of very large spans or for the cases where the deflection is critical. Also, as expected, the considerable member forces of rigid-joint dome show that this structure is stiffer than the pin-joint dome structure. On the other hand, it shows the high rigidity of the rigid-jointed connection domes. As another observatory, it is seen that the rigid-joint dome offers a more economical design. For example, by considering the mass density of element material equal to 7698 kg/m^3 (76.98 kN/m^3), the optimum weight of pin-jointed and rigid-jointed domes will be 6212.2 kg and 4807.40 kg, respectively. This clearly shows that the single layer lamella dome with pin-jointed connections is 29 % heavier than the one with rigid-jointed connections.

It can be seen from Fig. 10 that the stress ratios of elements in lamella dome with rigid-joints is significantly more than single layer lamella dome with pin-joint connections. For example the maximum stress ratio related to rigid-jointed dome is 0.87, while for the pin-jointed dome this value is 0.51.

In this case of loading which is considerably close to real condition of loading on domes (because the wind, dead and snow loads are considered simultaneously) the stress and displacement constraints are both active for dome with rigid-connection. While for the dome with pin-joint connections because of having less rigidity, only the displacement constraints are active and also the stress ratios are very small compared to their allowable value. Therefore, for satisfying the displacement constraints and not losing the stability of the dome, stronger sections are chosen by ECBO for pin-joint connection dome. These points are supported by the comparisons of the results provided in Table 7.

6.3 Optimum designs of the single layer rigid-jointed and pin-jointed lamella suspended dome by ECBO

Rigid connections are often employed in the construction of long span single-layer domes, because the load capacity of pin-connected single-layer domes is very low. However, pin connections are often used in double-layer lattice domes, because the additional layer can make more stiffen structure than single layer latticed dome structure. By using the tensegrity system, the suspended dome structure performs same as a double-layer dome structure. Therefore, it is possible to use pin-jointed connections in the construction of the suspended dome system.

The tensegrity system which is constructed of cables and struts stiffens the suspended dome structure. The stiffness come from the opposite force to the external gravity load. On the other hand, the moment that is induced by the external load opposites to the moment that is induced by the tensegrity system. The explanation is illustrated by using the simply supported beam that is depicted in Fig. 11. This also shows that the maximum bending moment of suspended dome which is a combined system is decreased. Exciting the tensegrity system helps the suspended dome to work like a double-layer dome. In short, tensegrity system have double function on domes, which are reducing the elements stress and joints displacement of the structure.

It is worthwhile to mention that the applied optimum pre-stressed force of tensegrity system (radial and hoop cable) must be large enough to prevent cable slack, but not so large to buckle the struts and also induce very large opposite moment compared to moment induced by external loads. Also, obviously if the cables slack, then the tensegrity system does not work and also the opposite moment will not induced.

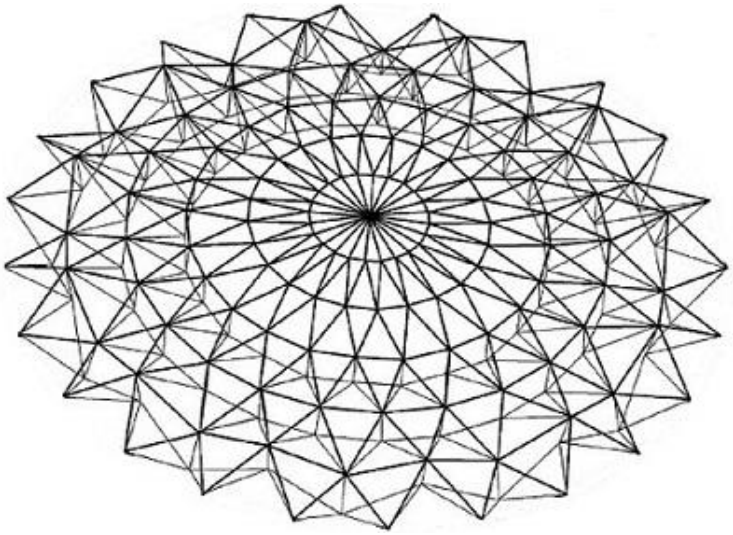

Fig. 11 Schematic of the lamella suspended dome with 6 rings

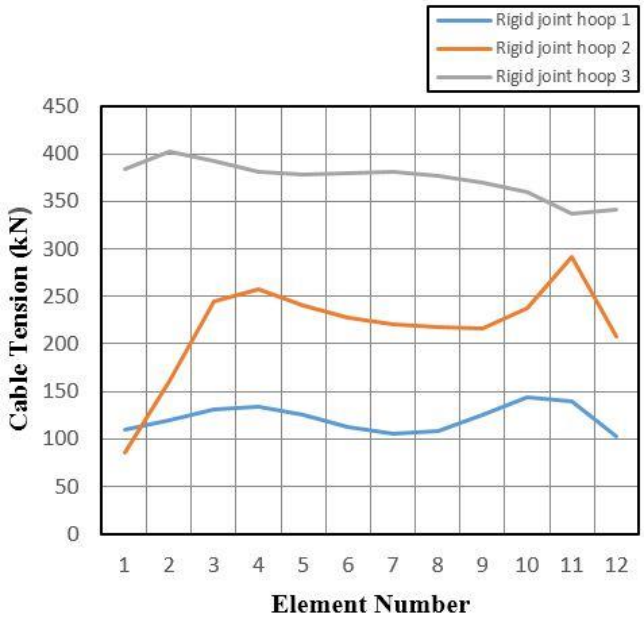

Fig. 12 Cable tension of hoop elements of the suspended dome with rigid-jointed upper layer

The six-ring suspended dome is employed as an example to illustrate this idea, Fig. 12. The computational model is a suspended dome having a span of 40 m. The top part of the model is a single-layer lamella dome, which has 6 rings and 12 joints in each ring. The single-layer lamella dome consists of steel tube beams that are fixed at both ends for suspended dome with rigid-jointed topmost layer and steel tube trusses for suspended dome with rigid-jointed topmost layer.

Its design tensile strength is 240 MPa. The material of cables is high strength wire, the technical parameters of these are provided in Table 2.

Table 8 Optimum design of upper single layer dome with pin-joint and rigid-joint connections. For lamella suspended dome using ECBO algorithm

		ECBO algorithm	
		Pin-joint	Rigid-joint
Number of rings		6	6
Optimum tubular	Group 1	PIPST(3)	PIPST(3)
Section designations	Group2	PIPST(8)	PIPST(8)
	Group 3	PIPST(10)	PIPST(8)
	Group 4	PIPST(10)	PIPST(8)
	Group 5	PIPST(8)	PIPST(4)
	Group 6	PIPST(10)	PIPST(8)
	Group 7	PIPST(10)	PIPST(10)
	Group 8	PIPST(8)	PIPST(5)
	Group 9	PIPST(10)	PIPST(10)
	Group 10	PIPST(8)	PIPST(8)
	Group 11	PIPST(10)	PIPST(5)
	Group 12	PIPST(8)	PIPST(4)
Height of crown (m)		3.50	3.50
Maximum displacement (cm)		2.79	2.80
$\sum l_I\ (m)$		974.04	974.04
$\overline{A}$ (cm^2)		54.64	39.28
Maximum strength ratio		52.34	74.57
Volume (m^3)		2.46	1.86

In this example the tensegrity system is constructed of three rings of hoop cables, radial cables and struts at the lower part of model. The tensegrity system connected to the rings 3, 4 and 5 of a single layer lamella dome by vertical struts elements. For example, the struts of group 1 are connected to the joints which are located in the third ring of the single layer lamella dome. The struts are compression elements and have hinged connection on both ends; its sections are circular steel tubes. The suspended domes structure is subjected to 0.8 kN/m^2 of dead load, 0.2 kN/m^2 of live load, and 0.2 kN/m^2 of basic wind pressure.

Optimal cable force is a function of the length of the struts, span-to-rise ratio and cross-sections of the cables. The internal force of the cables in pre-stressed steel structures is due to two factors, one is from the external loads, and the other is due to the tensioning of the cables.

When these suspended domes are compared, it is seen that the suspended dome with rigid-joint topmost layer offers a more economical design. For example, by considering the mass density of material equal to 7698 kg/m^3, the optimum weight of topmost layer with pin-joint and rigid-joint connection will be 18937.08 kg and 14318.28 kg, respectively. This clearly shows that for suspended domes, the topmost layer with pin-joint connections is 24.39 % heavier than the topmost layer with rigid-joint connections.

It can be seen from Table 8 that using the capacity of elements in suspended dome with rigid-joints is approximately 27 % more than the suspen-dome with pin-joint connections. In this case of loading which the wind, dead and snow loads are applied on the suspend dome and the diameter is two times bigger than the dome which discussed in the previous sections, displacement constraints is more active than the stress constraints for both types of suspended domes.

Table 9 Optimum design of tensegrity system of the suspended dome with upper layer pin-jointed and rigid-jointed connections obtained using the ECBO algorithm

		ECBO algorithm	
		Pin-joint	Rigid-joint
Number of hoop cable		3	3
Cable and section	Hoop 1	Cable (11.3)	Cable (9.6)
	Hoop 2	Cable (15.2)	Cable (15.2)
	Hoop 3	Cable (9.6+15.7)	Cable (15.7+8)
	Radial 1	Cable (8)	Cable (8)
	Radial 2	Cable (11.3)	Cable (11.3)
	Radial 3	Cable (15.2)	Cable (12.5)
	Strut 1	PIPST (1/2)	PIPST (1/2)
	Strut 2	PIPST (1/2)	PIPST (1/2)
	Strut 3	PIPST (3/4)	PIPST (3/4)
Initial strain		0.00050	0.00041
$\sum l_c(m)$		562.39	562.39
$\sum l_s(m)$		36	36
Hoop Cable Volume (m^3)		0.072	0.6343
Radial Cable Volume (m^3)		0.031	0.027
Strut Volume (m^3)		0.00611	0.00611

The length of the struts which are connected to rings number 3, 4 and 5 are obtained as 1.5, 1 and 0.5 for both suspended domes, respectively. Also, the total lengths of the struts of both suspended domes are identical. Obviously, large amount of strain energy and element forces are induced in the cables of tensegrity system and steel elements of the topmost layer. Therefore, the least area sections are obtained for struts elements according to Table 9.

When the tensegrity systems of suspended dome are compared, apart from struts elements which is discussed, it can be seen that cables system of suspended dome with upper layer rigid-joint is more economical and also has lighter design. For example, the optimum volume of hoop cable of pin-joint and rigid-joint suspended dome are obtained as 0.072 m^3 and 0.063 m^3, respectively, and also for radial cables these are obtained as 0.031m^3 and 0.027m^3. This shows that the tensegrity system cables of suspended dome with pin-jointed connections is 12.9 % heavier than the suspended dome of rigid-jointed connections.

As an another observatory, Fig. 13 shows that the forces in the hoop cable number 3 which is the outer hoop cable of tensegrity system is significantly more than those inner hoop cables and the existing forces in cable elements of the third hoop is the biggest. In short, it is essential to design and construct the tensegrity system, with its hoop cables being located in outer part of the system.

7. Conclusions

In this paper, the enhanced Colliding Bodies Optimization (ECBO) is utilized for optimum design of suspended dome with considering the type of element connections. The height of

suspended dome, the length of the strut, cables initial strain, the cross-sectional area of the cables and the cross-sectional size of steel members are considered as design variables and the volume of the entire structure as the objective function, an optimization method is proposed in the paper based on the enhanced colliding body optimization. For single layer lamella dome, this algorithm also determines the total number of rings, the number of nodes on each ring, the optimum height and the optimum steel section designations for the members of domes from the available steel pipe section table and implements the design constrains from LRFD-AISC. ECBO considers not only the strength of steel components and cables as constraints but also the stability of the steel members and the displacement of the overall structure.

A simple procedure is presented to calculate the joint coordinates and specify the elements to determine the configuration of single layer lamella dome and its suspended dome which is a spatial pre-stressed structure with complex mechanical characteristics. First, the joint coordinates are calculated. Then using some simple relationships, the steel elements, struts and cables are constructed.

A complete investigation on the efficiency of single layer dome considering pin-joint and rigid-joint connection under real loading condition is performed. Wind load, which has considerable effect on space structures, especially domes, is applied on single layer lamella dome according to ASCE 7-05. Dead or snow load conditions according to ANSI-A58, and also more realistic behavior of the dome is taken into account.

In suspended dome structure, tensegrity system significantly reduced the stresses and the displacements of structure. By using the tensegrity system, the suspended dome structure performs like a double-layer dome structure. Therefore, it is logical to use pin-connected joints in the construction of the suspended dome systems. However, it is seen that the suspended dome with upper layer rigid-joint offers a more economical design. The tension of outer hoop ring of tensegrity system of suspended dome is large and the tension of other cables is relatively small. Therefore, it is important to construct the tensegrity system, which its hoop cables being located in outer part of system.

The ECBO method which is one of the recent additions to stochastic search techniques of numerical optimization is used to obtain the solution of the design problems. It can be observed from the design examples of this study that the enhanced colliding body method can be used in finding the solution of optimum topology problem where the topology, shape and size of members in a structure are taken as design variables.

Acknowledgements

The first author is grateful to the Iran National Science Foundation for the support.

References

American Institute of Steel Construction (AISC) (1989), *Manual of steel construction allowable stress design*, 9th Edition, AISC, Chicago.

American National Standards Institute (ANSI) (1980), *Minimum design loads for buildings and other structures* (ANSI A58.1).

American Society of Civil Engineers (ASCE) (2006), *Minimum design loads for buildings and other*

structures (ASCE-SEI 7-05).
Chen, Z., He, Y., Wang, Z., Liu, H. and Wang, X. (2015), "Integral analysis of shallow ellipsoidal suspend-dome with elastic restraint", *Int. J. Space Struct*., **30**(1), 37-52.
Dorigo, M., Maniezzo, V. and Colorni, A. (1996), "The ant system: optimization by a colony of cooperating agents", *IEEE Tran. Syst. Man. Cyber. B*, **26**(1), 29-41.
Eberhart, R.C. and Kennedy, J. (1995), "A new optimizer using particle swarm theory", *Proceedings of the Sixth International Symposium on Micro Machine and Human Science*, Nagoya, Japan.
Erol, O.K. and Eksin, I. (2006), "New optimization method: Big Bang-Big Crunch", *Adv. Eng. Softw*., **37**, 106-11.
Fogel, L.J., Owens A.J. and Walsh, M.J. (1996), *Artificial intelligence through simulated evolution*, Wiley, Chichester.
Gonçalves, M.S., Lopez, R.H. and Miguel, L.F.F. (2015), "Search group algorithm: a new metaheuristic method for the optimization of truss structures", *Comput. Struct*., **153**, 165-184.
Holland, J.H. (1975), *Adaptation in natural and artificial systems*, University of Michigan Press, Ann Arbor, USA.
Kamyab, R. and Salajegheh, E. (2013), "Size optimization of nonlinear scallop domes by an enhanced particle swarm algorithm)", *Int. J. Civil Eng*., **11**(2), 77-89.
Kaveh, A. (2014), *Advances in metaheuristic algorithms for optimal design of structures*, Springer Verlag, Switzerland.
Kaveh, A. and Forhoudi, N. (2013), "A new optimization method: dolphin echolocation)", *Adv. Eng. Softw*., **59**, 53-70.
Kaveh, A. and Ilchi Ghazaan, M. (2014), "Enhanced colliding bodies optimization for design problems with continuous and discrete variables", *Adv. Eng. Soft*w., **77**, 66-75.
Kaveh, A. and Khayatazad, M. (2012), "A novel meta-heuristic method: ray optimization", *Comput. Struct*., **112-113**, 283-294.
Kaveh, A. and Mahdavai, V.R. (2014), "Colliding bodies optimization: a novel meta-heuristic method", *Comput. Struct*., **39**, 18-27.
Kaveh, A. and Mahdavai, V.R. (2015a), *Colliding bodies optimization; extensions and applications*, Springer Verlag, Switzerland.
Kaveh, A. and Mahdavi, V.R. (2015b), "Colliding bodies optimization for size and topology optimization of truss structures", *Struct. Eng. Mech*., **53**(5), 847-865.
Kaveh, A. and Rezaei, M. (2015), "Topology and geometry optimization of different types of domes using ECBO", *Adv. Comput. Des.* (in Press)
Kaveh, A. and Talatahari, S. (2010a), "A novel heuristic optimization method: charged system search", *Acta Mech*., **213**, 267-89.
Kaveh, A. and Talatahari, S. (2010b), "Optimal design of Schwedler and ribbed domes via hybrid Big Bang-Big Crunch algorithm", *J. Constr. Steel Res*., **66**, 412-419.
Kaveh, A. and Talatahari, S. (2010c), "Optimal design of single layer domes using meta-heuristic algorithms; a Comparative study", *Int. J. Space Struct*., **25**(4), 217-227.
Kaveh, A. and Talatahari, S. (2011), "Geometry and topology optimization of geodesic domes using charged system search", *Struct. Multidiscip. Optim*., **43**(2), 215-229.
Kawaguchi, M., Abe, M., Hatato, T., Tatemichi, I., Fujiwara, S. and Anma, Y. (1997), "Structural tests on a full-size suspended dome re", *Proceedings of IASS International Symposium on Shell and Spatial Structure*, Singapore, **1**, 431-438.
Kawaguchi, M., Abe, M. and Tatemichi, I. (1999), "Design, tests and realization of suspended dome system", *J. Int. Asso. Shell Spatial Struct*., **40**(3), 179-192.
Kociecki, M. and Adeli, H. (2013), "Two-phase genetic algorithm for size optimization of free-form steel space frame roof structures", *J. Construct. Steel Res*., **90**, 283-296.
Mirjalili, S. (2015), "The ant lion optimizer", *Adv. Eng. Softw*., **83**, 80-98.
Nie, G.B., Fan, F. and Zhi, X.D. (2013), "Test on the suspended dome structure and joints of dalian gymnasium", *Adv. Struct. Eng*., **16**(3), 467-486.

Sadollah, A., Eskandar, H., Bahreininejad, A. and Kim, J.H. (2015), "Water cycle, mine blast and improved mine blast algorithms for discrete sizing optimization of truss structures", *Comput. Struct.*, **149**, 1-16.
Saka, M.P. (2007), "Optimum geometry design of geodesic domes using harmony search algorithm", *Adv. Struct. Eng*., **10**(6), 595-606.
Saka, M.P. and Geem, Z.W. (2013), "Mathematical and met heuristic applications in design optimization of steel frame structures: an extensive review", *Math. Prob. Eng*., Article ID 271031.
Wang, Z., Wang, X., Chen, Z. *et al.* (2015), "Suspend-dome structure design and analysis for steel roof of bicycle gymnasium in Tianjin Sports Center", *Build. Struct.*, **45**(5), 6-9.
Yan, X., Yu, J., Ma, S. *et al.* (2015), "Analysis and design of suspendome structure roof of Qinyang Gymnasium", *Build. Struct*., **45**(3), 6-9.
Zhengrong, J., Wang, S.., Shi, K. *et al.* (2013), "Nonlinear buckling analysis of long-span elliptic paraboloid suspended dome structure for Houjie Gymnasium", *Chin. Civil Eng. J.*, **45**(2), 21-28.

CC